Performance characteristics of a passive direct formate fuel cell

Xiangyu Su, Zhefei Pan, Liang An*

Department of Mechanical Engineering, The Hong Kong Polytechnic University, Hung Hom, Kowloon, Hong Kong SAR, China.

*Corresponding author.

Email: liang.an@polyu.edu.hk (L. An)

Abstract

A passive direct formate fuel cell using ambient air is designed, fabricated and tested. This fuel cell does not use any auxiliary devices such as pumps, gas compressors, and gas blowers. The simple and compact structure well fits the need of portable applications. In this fuel cell, formate in an alkaline solution is used as anode fuel, while ambient oxygen is used as cathode oxidant, and a cation exchange membrane serves as an ionic conductor between two electrodes. Our performance tests have shown that a peak power density of 16.6 mW cm^{-2} as well as an open-circuit voltage of 0.97 V are achieved by the present fuel cell at 60 ^{o}C, when running on anode fuel containing 5.0 M sodium formate and 3.0 M sodium hydroxide. This performance is even 31.7 % higher than that achieved by an active direct formate fuel cell reported in the open literature (12.6 mW cm^{-2}), which also uses a cation exchange membrane. The effects of the operating parameters are also investigated, including the concentrations of fuel and alkali in the anode fuel as well as the operating temperature. The fuel solution at low concentrations results in an inadequate local concentration of reactants in the anode catalyst layer, so that the anodic kinetics becomes sluggish. Although increasing the sodium hydroxide concentration enhances the anodic formate oxidation kinetics, too high concentration of sodium hydroxide leads to too many active sites being covered by hydroxide ions and thus adsorption and reaction of formate ions being limited. Moreover, too high concentration of sodium hydroxide or sodium formate also leads to the fuel solution being

highly viscous, hindering the motion of various ions, as well as thus increasing both concentration loss and the ohmic loss. The compromise between benefits and the drawbacks of using high-concentration reactants results in an optimal composition of the fuel solution, which contains 5.0 M sodium formate and 3.0 M sodium hydroxide. Furthermore, the present fuel cell delivers a voltage around 0.6 V for 20 hours at 4.0 mA cm^{-2}.

Keywords: Passive; direct formate fuel cells; air-breathing cathode; operating parameters; power density

1. Introduction

Worldwide attention has been drawn by fuel cells, which generate electricity via electrochemical oxidation of fuel and reduction of oxygen, primarily due to their high efficiencies and environmentally friendly characteristics [1-4]. The potential fuels can be gaseous hydrogen and liquid fuels, *i.e.*, methanol, ethanol, formic acid, formate etc., while the fuel selection dominates the fuel cell performance, environmental impact, operation safety, and cost. Generally, the fuel cell using hydrogen can yield a high performance, due to the extremely fast hydrogen oxidation kinetics and the clean product, water (zero emission). However, the intrinsically explosive nature of hydrogen gives rise to the safety issue and increases the cost on storage, transportation, and handling. The high operation cost of hydrogen limits the practical application of hydrogen fuel cells [5-7]. For this reason, liquid fuels have gained more attention, primarily because of their high energy densities and easier-operated characteristics [8-18]. Among them, formate, mainly referring to sodium formate (HCOONa) or potassium formate (HCOOK) dissolved in an aqueous solution, has drawn increasing interest due to the following advantageous characteristics: (1) the theoretical voltage of direct formate fuel cells (DFFCs) running on oxygen is 1.45 V, which exceeds 1.21 V of direct methanol fuel cells, 1.14 V of direct ethanol fuel cells and 1.09 V of direct ethylene glycol fuel cells; (2) solid formate salts can be easily stored, transported and handled, and they have high melting points (253 ^{o}C of sodium formate and 167.5 ^{o}C of potassium formate) so that they are ready for extensive use; (3) the fuel solution can be easily formed via dissolving formate salts into water; (4) formate salts can be synthesized through photoelectrochemically reducing carbon dioxide, along with solar energy harvesting [19]; (5) formate oxidation reaction (FOR) is facile in alkaline media [20, 21]; and (6) radically different from incomplete oxidation of ethanol producing acetic acid and water, formate can be fully oxidized producing water and carbon dioxide, resulting in high electron transfer rate

and current efficiency [22, 23]. Therefore, DFFCs have been extensively investigated and remarkable progress has been made [24-33]. Bartrom et al. [24] fabricated a DFFC, which employed a Pd black painted carbon cloth as the anode, a Pt black painted carbon cloth as the cathode, as well as an anion exchange membrane (AEM). This fuel cell exhibited a peak power density (PPD) of 144 mW cm^{-2} at 60 ºC with anode fuel flow with 2.0 M potassium formate and 2.0 M potassium hydroxide fed at a flow rate of 1.0 mL min^{-1} and a pure oxygen flow at 100 sccm. They, Bartrom et al. [25], further optimized the anode fabrication method and found that this fuel cell performance was much improved to a PPD of 267 mW cm^{-2} at 60 ºC with the same fuel and oxidant supply. Nguyen et al. [26] proposed and investigated a Pt-free DFFC, which employed a Pd black painted carbon cloth as the anode, a commercial Fe-Co catalysts painted carbon paper as the cathode, as well as an AEM as electrolyte membrane. A PPD of 35 mW cm^{-2} was delivered by this fuel cell at 20 ºC, with an anode fuel flow having 1.0 M potassium formate and 2.0 M potassium hydroxide at the same flow rate as well as an air flow (flow rate: 400 sccm). Zeng et al. [27] prepared a home-made quaternized polysulfone membrane and assembled a DFFC using this as-prepared membrane with a Pd/C painted nickel foam as the anode and a Fe-Co catalysts painted carbon paper as the cathode. The fuel cell showed a PPD of 250 mW cm^{-2} at 80 ºC, with an anode fuel flow containing 1.0 M potassium formate and 2.0 M potassium hydroxide as well as a pure oxygen flow. Li et al. [28] constructed a unique DFFC using Nafion 211 membrane as cation exchange membrane (CEM) and a pair of Pd/C painted carbon paper as electrodes, which was able to produce electricity and base simultaneously. The maximum current density reached 210 mA cm^{-2} and a PPD of 36 mW cm^{-2} was achieved at 80 ºC with an anode fuel flow containing 2.0 M sodium formate and a pure oxygen flow. Li et al. [29] presented and studied a DFFC replacing the oxygen with hydrogen peroxide, which employed two pieces of Pd-Au alloy coated nickel foam as electrodes and an AEM. This fuel cell yielded a PPD of 331 mW cm^{-2}

at 60 ºC, when operated on an anode fuel flow having 1.0 M HCOONa and 2.0 M NaOH and a cathode oxidant flow having 1.0 M H_2O_2 and 1.0 M H_2SO_4. After that, Li et al. [30] tested the performance of a formate-peroxide fuel cell without adding an alkali. This fuel cell was consisting of a Pd/C coated carbon paper as the anode, a Pt/C coated carbon paper as the cathode, as well as an AEM. This alkali-free formate-peroxide fuel cell output a PPD of 38 mW cm^{-2} at 40 ºC, with an anode fuel flow having 7.0 M potassium formate and an oxidant solution flow containing 15 wt.% hydrogen peroxide (flow rate: 3.0 mL min^{-1}). The performance characteristics of formate-peroxide fuel cells was comprehensively investigated by Li et al. [31]. The effects of catalyst loadings, solution compositions and other operating parameters on the fuel cell performance were examined. The optimal parameters were found to be 2.0 mg cm^{-2} Pd loading at the anode, 2.0 mg cm^{-2} Pt loading at the cathode, 1.0 M sodium formate and 3.0 M sodium hydroxide in the fuel solution, as well as an operating temperature of 60 ºC, respectively. The PPD was 600 mW cm^{-2} at 60 ºC. In addition, some other innovative compact and passive designs were fabricated and demonstrated [32, 33]. Copenhaver et al. [32] proposed and tested a microfluidic paper‐based DFFC. This DFFC was constructed in a "back-to-back" in-series dual-cell configuration. Each single cell was composed of a paper substrate, a Y‐shaped microfluidic flow field, 3‐mm diameter Pd/C dots at the anode and 3‐mm diameter colloidal graphite at the cathode. The total Pd loading on each paper was 0.2 mg cm^{-2}. The flows of fuel solution and oxidant solution can be driven by the capillary force that eliminates any external pumps. This microfluidic DFFC resulted in a PPD of 2.5 mW mg^{-1} Pd at room temperature, when operated on an anode fuel flow having 5.0 M HCOOK and 1.0 M KOH, as well as an oxidant solution flow containing 30 wt. % H_2O_2 and 1.0 M HCl. In addition, the microfluidic DFFC still resulted in a voltage of approximately 0.5 V at a current of 1.0 mA for 15 mins after stopping the electrolyte flow. After that, Galvan et al. [33] further improved this microfluidic paper‐based DFFC via

optimizing the following design parameters: i) width and length of the flow field, ii) materials of the current collector, and iii) mass ratios of carbon in the composite catalyst. After optimization, three DFFCs were fabricated and connected in series to work as power sources for several LED lights and a handheld calculator.

From the literature review, it can be seen that the pervious investigations were mainly focused on active DFFCs, which have to use liquid pumps and gas blowers/compressors to supply the fuel solution and oxygen/air [24-31]. Although the fuel cell performance in an active mode is attractive, they require additional space and controllers for pumps and blowers/compressors, making the fuel cell system bulky and heavy. Passive fuel cells, which eliminate any use of pumps or gas compressors/blowers and thus possess the simple and compact design, ~~which~~ is suitable for powering portable electronic devices. In this work, we design and fabricate a passive formate fuel cell employing a Pd/C coated carbon cloth as the anode, a Fe-Co catalyst coated carbon cloth as the cathode, and a CEM as solid electrolyte. In addition, we further examine and understand the effects of the compositions of the fuel solution and the operating temperature on the fuel cell performance.

2. Working principle of the passive DFFC

The proposed passive fuel cell is consisting of a fuel reservoir, an anode, a CEM, an air-breathing cathode, a pair of current collectors and a window-opened plate for air breathing, as shown in Figure 1. Before discharging, the fuel reservoir is filled with the fuel solution containing HCOONa and NaOH. It has been demonstrated that NaOH is not essentially added, because the hydrolysis of HCOONa can generate a considerable amount of OH^- ions in the aqueous solution for the FOR as well. During operation, formate ions ($HCOO^-$) and hydroxide ions (OH^-) transport, driven by the concentration gradient, initially from the bulk solution finally to the anode catalyst layer via the current collector as well as the diffusion

layer. The FOR occurs on the anode active sites of the nanoparticles, in which formate ions are oxidized to generate water and carbonate, as well as electrons, as expressed by [34]:

$$HCOO^- + 3OH^- \rightarrow CO_3^{2-} + 2H_2O + 2e^- \qquad E^0_{FOR} = -1.05\ V \qquad (1)$$

The produced electrons are transported through the external circuit and received by the cathode. On the cathode, electrons, oxygen and water participate in the oxygen reduction reaction (ORR) to produce OH^- ions as [26]:

$$2H_2O + O_2 + 4e^- \rightarrow 4OH^- \qquad E^0_{ORR} = 0.40\ V \qquad (2)$$

Meanwhile, Na^+ is transferred from the anode to cathode via the CEM, forming the internal ionic circuit. It should be mentioned that sodium ions crossing the membrane could also bring water to the cathode due to the electro-osmosis drag, in addition to water crossover via diffusion. Consequently, the combination of Equation (1) and Equation (2) results in the overall reaction:

$$2HCOO^- + 2OH^- + O_2 \rightarrow 2CO_3^{2-} + 2H_2O \qquad E^0 = 1.45\ V \qquad (3)$$

The theoretical voltage of the passive DFFC is 1.45 V, which greatly exceeds that of direct methanol fuel cells (1.21 V) [35], direct ethanol fuel cells (1.14 V) [36, 37], and direct ethylene glycol fuel cells (1.09 V) [9]. However, it should be also mentioned that in fuel cells, the theoretical one is hardly achieved due to overpotentials in physical and chemical processes [8-18]. First, the open-circuit voltage (OCV) is lower than the theoretical value due to the poor reversibility of electrode reactions [38]. Second, the fuel crossover will induce the mixed potential in the cathode, which further lowers the cell voltage [15]. Third, during discharging, the voltage will be further decreased, due to the activation loss, ohmic loss and concentration loss at a given current density.

3. Experiments

3.1. Preparation of the membrane electrode assembly

A membrane electrode assembly (MEA) was prepared with an active area of 2.0 cm × 2.0 cm. It is consisting of two home-made electrodes, and a CEM (a pretreated Nafion 211 membrane). The anode was prepared by a layer of Pd/C catalyst (30 wt. %, Sigma-Aldrich) sprayed onto a diffusion layer made of a hydrophilic carbon cloth (Hesen, China), with a loading of 1.0 mg_{Pd} cm^{-2}. The fabrication process [31] is described as follows: i) an ink was prepared by blending Pd/C catalysts with 5 wt. % Nafion solution (Fuel Cell Store, USA), and an appropriate amount of ethanol as the solvent, followed by continuously stirring in a 20-minute ultrasonic bath to well disperse the catalysts and ionomer. ii) The ink was then sprayed onto the hydrophilic carbon cloth by an air spray gun, and the electrode was dried in the ambient air. The cathode was fabricated by brushing carbon supported Fe–Co catalysts (K-14 HYPERMEC, ACTA) on a hydrophobic carbon cloth (ETEK) [35], with a metal loading of 1.0 mg cm^{-2}. Prior to the fuel cell assembly, a Nafion 211 membrane, which was received in H^+ form, was pretreated to form the CEM, which was in Na^+ form, by the approach reported previously [39]: i) a 10 wt. % NaOH aqueous solution was prepared; ii) the membrane was immersed in the aqueous solution; iii) the solution was heated to 80 ºC using a hot plate; and iv) after one-hour treatment, the membrane was washed by deionized (DI) water to remove the residual NaOH. The as-prepared CEM was immersed in DI water before the use.

3.2. Experimental setup

It is seen from Figure 2 that the fuel cell system was constructed by the following components: a window plate, a cathode current collector, an MEA, an anode current collector, a reservoir plate, and an end plate. The end plate, reservoir plate and window plate were made of stainless steel 1Cr18Ni9Ti, while two current collectors were made of stainless steel 316L. The polytetrafluoroethylene (PTFE) gaskets with the appropriate thicknesses were placed between the components to avoid the liquid leakage. The inner face of the end plate

was covered by a PTFE sheet, and the screws were covered by polyvinyl chloride (PVC) insulation pipes, in order to prevent the short circuit. In the reservoir plate, two holes were drilled: i) one hole was reserved for placing a heating rod to heat up the fuel cell; ii) the other hole was drilled through to the solution reservoir for injecting the fuel solution into the reservoir. The current collectors, which have 25 holes with the same diameter of 3.2 mm, were manufactured by laser-cutting technique. The holes allow reactants and products to transport between the electrode and the reservoir/the ambient air.

3.3. Test instrumentation

The tests, including: 1) polarization curve; 2) internal resistance via current interrupt method [40]; 3) OCV; and 4) constant-current discharging were conducted with an Arbin BT2000 (Arbin, USA). In addition, the Electrochemical impendence spectra (EIS) test was conducted with a CHI 605C (CH Instruments, China). A temperature controlling system was used to regulate the operating temperate, which was constructed as follows: i) a heating rod was installed in the reservoir plate; ii) a thermocouple was placed through the injection hole; and iii) a temperature controller works based on the feedback of the thermocouple.

4. Results and discussion

4.1. General performance

Figure 3 shows the polarization and power density curves of the present passive DFFC, when it was running with a fuel flow containing 5.0 M HCOONa and 3.0 M NaOH at 60 ºC. It is found that the OCV was 0.97 V and the PPD was 16.6 mW cm^{-2}. The OCV (0.97 V) was 0.48 V lower than the theoretical voltage (1.45 V), which is ascribed to the poor reversibility of the anodic and cathodic reactions. The PPD achieved by this passive DFFC is even higher than an active DFFC (12.6 mW cm^{-2}) [41], which employed 2.0 mg cm^{-2} Pd/C in the anode and 2.0 mg cm^{-2} Pt/C in the cathode with a pretreated CEM (Nafion 117, thickness: 117.8 μm) at 60 ºC. The performance improvement is primarily due to the use of a thinner membrane

(Nafion 211, thickness: 25.4 μm), resulting in a lower ohmic loss. It should also be mentioned that an active DFFC proposed by Li et al. [28] resulted in the maximum current density of 210 mA cm^{-2} and the PPD of 36 mW cm^{-2} at 80 ºC. Figure 4 displays the transient discharging behavior of the present fuel cell at 4.0 mA cm^{-2} at 23 ºC. It is demonstrated that the present fuel cell can discharge for 20 hours with a stable voltage around 0.6 V. The discharging voltage (0.6 V) was drawn down by 0.37 V from the OCV (0.97 V), which was attributed to three losses mentioned above at a given current density (4.0 mA cm^{-2}). This discharging performance exhibits the feasibility for practical applications of this fuel cell. For the given design, elevating the feeding concentrations of reactants in the fuel reservoir will increase the reactant concentrations in the catalyst layer, which is called local concentrations. Within a certain increase range, the anodic reaction kinetics will be enhanced due to the increase of local reactant concentrations [42, 43], the internal resistance will be lowered as the increase of ionic conductivity of the membrane [44], and the energy capacity will be increased due to an increase of the fuel amount. However, the previous investigations on liquid fuel cells have demonstrated that too high concentration will lead to some drawbacks due to i) species crossover, meaning that formate and alkali can pass through the membrane and reach the cathode, resulting in the mixed potential and a waste of species, as well as lowering the cathodic kinetics [45]; ii) competitive adsorption, meaning that when one reactant is excessive, the adsorption of the other on active sites will be limited [46]; and iii) higher solution viscosity, increasing transport resistances of various reactants [47]. Another parameter, the operating temperature, can also affect the transport process and the fuel cell performance. For example, both the mass transport and reaction kinetics will be enhanced at elevated temperatures, but the species crossover rate will be increased as well. Therefore, it is significantly critical to investigate how the operating parameters affect the fuel cell performance.

4.2. Effect of the NaOH concentration

Figure 5 presents the polarization and power density curves when it was running on the fuel solutions containing 3.0 M HCOONa and various NaOH concentrations (0, 1.0, 3.0, 5.0 and 7.0 M) at 23 ºC. The addition of an alkali into the fuel solution can create a strong alkaline environment, which improves the ionic conductivity of the membrane, and further enhances the anodic kinetics. It should be mentioned that during preparation of the fuel solution, we could prepare the fuel solution having 3.0 M HCOONa and a limited NaOH concentration up to 7.0 M. When NaOH concentration increased to 9.0 M, it was found that NaOH cannot be fully dissolved in the aqueous solution. As such, the solubility of NaOH in 3.0-M HCOONa aqueous solution should be between 7.0 M and 9.0 M. The cell voltage increased with the NaOH concentration from 0 M to 3.0 M, and the maximum current density was increased from 42.5 to 52.5 mA cm^{-2}. Further increasing the NaOH concentration caused a decrease in the cell voltage, and the maximum current density was decreased to 25.0 mA cm^{-2}. As a result, for a given formate concentration, optimal NaOH concentration of 3.0 M yielded the highest PPD of 10.8 mW cm^{-2}, as shown in Figure 5.

The OCV and PPD achieved by the present fuel cell were 0.86 V and 5.1 mW cm^{-2}, respectively, even no alkali in the fuel solution. The low performance primarily resulted from the absence of NaOH, leading to the catalyst layer being starving for OH^- ions and thus the FOR kinetics being sluggish. Such sluggish FOR kinetics can also be demonstrated by the low OCV and the dramatic decrease of the cell voltage at 0 ~ 3.0 mA cm^{-2}. Adding NaOH into the fuel solution can significantly enhance the FOR kinetics. As indicated in Figure 6, with the increase in the NaOH concentration from 0 to 1.0 M, the OCV was raised from 0.86 V to 0.99 V. In addition, the cell voltage in the whole current density range was higher than that achieved by the alkali-free operation as presented in Figure 5. The improvement was ascribed to the enhanced FOR kinetics by adding an alkali. At current densities higher than

25 mA cm^{-2}, the voltage increment was much smaller since the higher consumption rate of OH^- ions caused the low local concentration of OH^- ions and thus the enhancement of the FOR kinetics was limited. When the NaOH concentration was increased to 3.0 M, the cell voltage was further increased. The explanation for this phenomenon requires the understanding on the OCV behavior in Figure 6. It is found that, although increasing the NaOH concentration from 1.0 M to a higher concentration decreased the OCV by around 30 mV, the OCV with alkali was still 100-130 mV higher than that achieved by the alkali-free operation. Hence, it can be concluded that the excessive condition was more beneficial to the FOR kinetics than the inadequate one. With 1.0 M NaOH, the local concentration of OH^- ions was much lower than 1.0 M due to the consumption by the anodic reaction. The inadequate local concentration of OH^- ions caused poor FOR kinetics. When the NaOH concentration was 3.0 M, the local concentration OH^- ions was sufficient, so that the FOR kinetics was much enhanced and thus the fuel cell performance was improved. Moreover, the composition of the fuel solution (HCOONa:NaOH=1:1) caused the local concentration ratio being close to the consumption ratio based on the overall reaction, as indicated by Equation (3). The appropriate ratio of two reactants results in the proper adsorption.

The alkaline environment significantly influences the anodic kinetics as well as the transport of reactants to active sites. It can be seen that further increasing the NaOH concentration to 7.0 M decreased the fuel cell performance: the PPD was decreased to 9.3 and 9.0 mW cm^{-2}, respectively, and the maximum current density was dramatically decreased to around 25 mA cm^{-2}. The degradation was attributed to two aspects: i) the FOR kinetics was hindered, as indicated by the OCV behavior in Figure 6. This is because the excessive OH^- ions occupied too many active sites and thus limited the adsorption and reaction of $HCOO^-$ ions; ii) more importantly, too high NaOH concentration also greatly increased the solution viscosity [47], increasing the transport resistance of various ions, evidenced by the internal resistance

behavior in Figure 6. In summary, there is an optimal NaOH concentration of 3.0 M resulting in the best fuel cell performance.

4.3. Effect of the HCOONa concentration

Figure 7 shows the polarization and power density curves when it was running on the fuel solutions containing 3.0 M NaOH and various HCOONa concentrations (1.0, 3.0, 5.0 and 7.0 M) at 23 ^{o}C. It can be seen that the fuel cell performance was upgraded with increasing the HCOONa concentration from 1.0 M to 5.0 M, while further increasing the concentration to 7.0 M degraded the fuel cell performance. It is shown that 1.0-M operation yielded a PPD of 6.8 mW cm^{-2} and a maximum current density of 18.0 mA cm^{-2}. The low performance was attributed to the inadequate local concentration of $HCOO^-$ ions due to low concentration of $HCOO^-$ ions in the fuel solution and thus poor FOR kinetics. When the HCOONa concentration was increased to 3.0 M, the local concentration of $HCOO^-$ ions i was dramatically increased, resulting in the PPD being increased to 10.8 mW cm^{-2} and the maximum current density being increased to around 55.0 mA cm^{-2}. This is because increasing the local concentration of $HCOO^-$ ions enhances the FOR kinetics, which can be confirmed by the fact that the OCV was monolithically increased with the HCOONa concentration, as shown in Figure 8. When the HCOONa concentration was increased to 5.0 M, the cell voltage was almost the same with 3.0-M operation between 0 and 20.0 mA cm^{-2}. At current densities between 20.0 and 35.0 mA cm^{-2}, the cell voltage was higher than that achieved by the 3.0-M operation, but it became lower than the 3.0-M operation at current densities higher than 35.0 mA cm^{-2}. The higher cell voltage in the moderate current density range was attributed to the increased local concentration of $HCOO^-$ ions, which further improved the FOR kinetics. The lower cell voltage was because that the higher HCOONa concentration increased the viscosity of the fuel solution and thus the transport resistance of various ions was increased [47]. When the HCOONa concentration was further increased to 7.0 M, the

transport resistance was further increased and thus the fuel cell performance was even worse. The increased transport resistance can be evidenced by the internal resistance behavior in Figure 8. In summary, there is an optimal HCOONa concentration of 5.0 M resulting from the tradeoff between upgrading the mass transport of $HCOO^-$ ions and degrading the anodic kinetics.

4.4. Effect of the operating temperature

It is indicated in Figure 9 that the fuel cell performance was monolithically upgraded with the operating temperature. The peak power densities achieved at temperatures of 23, 40 and 60 ^oC were 9.9, 13.6 and 16.6 mW cm^{-2}, respectively. The OCV was decreased slightly when it increased from 40 to 60 ^oC. This indicates that fuel crossover became significant at 60 ^oC. The micro-channels of the membrane were expanded at high temperatures and then the permeability for HCOONa was increased [48, 49]. The presence of HCOONa in the cathode induced the FOR occurring on the Pt surface and thus the mixed potential on the cathode, decreasing the cell voltage. Despite of the decrease in the OCV, almost in the whole discharging current density range, the cell voltage was still increased with higher operating temperature. The reasons for this phenomenon are as follows: 1) high-temperature operation accelerates the adsorption and desorption of reactants/products on active sites, thereby enhancing the reaction kinetics of both anode and cathode; and 2) In this fuel cell, the transport of various ions is predominated by diffusion and migration. Diffusivities and mobilities of various ions are highly temperature-dependent so that the concentration and ohmic losses will be reduced with higher temperature.

4.5. Constant-current discharging behavior

In practical applications, the power sources are required to deliver the stable voltage for hours or days, so that the long-term discharging stability should be guaranteed. Figure 10 shows the constant-current discharging behaviors of this passive fuel cell under different conditions. For

each discharging, the fuel cell was refueled with a 4.0-mL fuel solution. When the fuel solution had 1.0 M HCOONa and 3.0 M NaOH a, the passive DFFC could discharge for 7 hours with a significant voltage decay at 4.0 mA cm^{-2}. When elevating the HCOONa concentration to 5.0 M, the voltage was quite stable at around 0.6 V for 20 hours, although the voltage was decreased to 0.1 V in the next 15 hours. However, when the current density was increased to 8.0 mA cm^{-2}, the voltage stabilization time was shortened to 5 hours, and the output voltage was decreased to 0.45 V. An electrochemical reaction in fuel cells generally involves five steps: i) transport of the reactants from the bulk solution to the active sites, ii) adsorption of the reactants onto the active sites, iii) charge transfer between the reactants and the active sites (electrochemical reaction), iv) desorption of the products from the active sites, and v) transport of the products from the active sites to the bulk solution. In the discharging tests, the desorption of the products was slower than the adsorption of the reactants, the active sites could not be freed up to occupy the reactants, thereby blocking the adsorption of the reactants and causing the voltage decay. In addition, the products were accumulated in the catalyst layer, which hindered the transport of reactants, while the concentrations of reactants in the fuel solution were decreased due to the continuous consumption, therefore the local concentrations of reactants were decreased as well during the discharging. The decrease in both available active sites and local concentrations of reactants caused the voltage decay. When discharging with 1.0-M HCOONa, the local concentration of $HCOO^-$ ions became extremely low in a relatively short time, so that the discharging duration was short. When discharging with 5.0-M HCOONa, the local concentration of $HCOO^-$ ions in the catalyst layer was still sufficient in the considerable duration, resulting in a long discharging time. When the discharging current density was increased to 8 mA cm^{-2}, the consumption rate of reactants and the accumulation rate of products became faster, so that the FOR kinetics was dramatically degraded, and the discharging duration was much shortened. In summary,

increasing the feeding concentration and lowering the consumption rate (i.e., discharging current density) of HCOONa results in a stable discharging performance. The present fuel cell is capable of delivering a stable voltage around 0.6 V for more than 20 hours at 4.0 mA cm^{-2}, demonstrating the feasibility of this passive fuel cell for practical applications.

4.6. EIS analysis

The behavior of the polarization curves with the change of NaOH concentration was further examined by the EIS test. Figure 11 depicts the Nyquist plots of the of this present DFFC at various NaOH concentrations. In the high-frequency region, the impedance is dominated by the ohmic resistance and charge transfer resistance of the electrochemical reaction; while in the low-frequency region, the impedance is dominated by the mass transport [50]., it is seen from Figure 11 that when the NaOH increased from 0 M to 1.0 M, the arc of the impedance spectra shrank in the high-frequency region. When the NaOH concentration was further increased to 3.0, 5.0 and 7.0 M, the diameter was increased monolithically. This behavior further confirms that the charge transfer of the electrochemical reaction was enhanced with an added alkali, but it was retarded when the NaOH concentration increased to higher than 1.0 M due to the competitive adsorption. It is also found that the ohmic resistance was increased with the NaOH concentration. In the whole frequency range, it is indicated that the impedance was significantly increased with the NaOH concentration. The results confirm that although the electrochemical reaction was accelerated by an added alkali, too high concentration will increase the ohmic resistance and the mass transport resistance of the other reactant (formate). Therefore, there is an optimal NaOH concentration resulting in the best fuel cell performance.

5. Concluding remarks

In this work, a direct formate fuel cell using a cation exchange membrane is designed, fabricated and investigated. Effects of the composition of the fuel solution and the operating

temperature on the fuel cell performance are examined. It is shown that the peak power densities of the present passive direct formate fuel cell can reach 10.8 mW cm^{-2} and 16.6 mW cm^{-2} at 23 ^{o}C and 60 ^{o}C, respectively, when running on a fuel solution having 5.0 M HCOONa and 3.0 M NaOH. In addition, the present fuel cell can deliver a stable voltage of around 0.6 V for 20 hours at 4.0 mA cm^{-2}. While reducing the HCOONa concentration to 1.0 M or increasing the discharging current density to 8.0 mA cm^{-2}, the discharging duration is decreased to around 10 hours. This passive formate fuel cell does not use any auxiliary devices, such as pumps, gas blowers and gas compressors resulting in a simple and compact structural design. Hence, it is a promising power source for practical applications in portable electronic devices, such as mobile phones, laptops and drones.

Acknowledgement:

This work was fully supported by a grant from the Research Grants Council of the Hong Kong Special Administrative Region, China (Project No. 25211817).

References

[1] Z. F. Pan, L. An, T. S. Zhao, Z. K. Tang, Advances and challenges in alkaline anion exchange membrane fuel cells, Progress in Energy and Combustion Science 66 (2018) 141-175.

[2] I. Staffell, D. Scamman, A. V. Abad, P. Balcombe, P. E. Dodds, P. Ekins, N. Shahd, K. R. Ward, The role of hydrogen and fuel cells in the global energy system, Energy & Environmental Science 12 (2019) 463-491.

[3] Y. Wang, K. S. Chen, J. Mishler, S. C. Cho, X. C. Adroher, A review of polymer electrolyte membrane fuel cells: Technology, applications, and needs on fundamental research, Applied Energy 88 (2011) 981-1007.

[4] J. H. Wee, Applications of proton exchange membrane fuel cell systems, Renewable and Sustainable Energy Reviews 11 (2007) 1720-1738.

[5] D. K. Ross, Hydrogen storage: The major technological barrier to the development of hydrogen fuel cell cars, Vacuum 80 (2006) 1084-1089.

[6] D. Mori, K. Hirose. Recent challenges of hydrogen storage technologies for fuel cell vehicles, International Journal of Hydrogen Energy 34 (2009) 4569-4574.

[7] M. Felderhoff, C. Weidenthaler, R. V. Helmolt, U. Eberle. Hydrogen storage: the remaining scientific and technological challenges, Physical Chemistry Chemical Physics 9 (2007) 2643-2653.

[8] L. An, T. S. Zhao, R. Chen, Q. X. Wu, A novel direct ethanol fuel cell with high power density, Journal of Power Sources 196 (2011) 6219-6222.

[9] L. An, T. S. Zhao, S. Y. Shen, Q. X. Wu, R. Chen, Performance of a direct ethylene glycol fuel cell with an anion-exchange membrane, International Journal of Hydrogen Energy 35 (2010) 4329-4335.

[10] L. An, T. S. Zhao, S. Y. Shen, Q. X. Wu, R. Chen, Alkaline direct oxidation fuel cell with non-platinum catalysts capable of converting glucose to electricity at high power output, Journal of Power Sources 196 (2011) 186-190.

[11] Y. S. Li, T. S. Zhao, Ultra-low catalyst loading cathode electrode for anion-exchange membrane fuel cells, International Journal of Hydrogen Energy 37 (2012) 15334-15338.

[12] Y. S. Li, T. S. Zhao, A passive anion-exchange membrane direct ethanol fuel cell stack and its applications, International Journal of Hydrogen Energy 4 (2016) 20336-20342.

[13] Y. S. Li, T. S. Zhao, Z. X. Liang, Performance of alkaline electrolyte-membrane-based direct ethanol fuel cells, Journal of Power Sources 187 (2009) 387-392.

[14] Y. S. Li, T. S. Zhao, J. B. Xu, S. Y. Shen, W. W. Yang, Effect of cathode micro-porous layer on performance of anion-exchange membrane direct ethanol fuel cells, Journal of Power Sources 196 (2011) 1802-1807.

[15] Q. X. Wu, L. An, X. H. Yan, T. S. Zhao, Effects of design parameters on the performance of passive direct methanol fuel cells fed with concentrated fuel, Electrochimica Acta 133 (2014) 8-15.

[16] Q. X. Wu, T. S. Zhao, R. Chen, L. An, A sandwich structured membrane for direct methanol fuel cells operating with neat methanol, Applied Energy 106 (2013) 301-306.

[17] K. M. Arif, H.B. Zhao, W.W. Zou, Z. Chen, W.J. Cao, J.H. Fang, J.Q. Xu, L. Zhang, J.J. Zhang, Recent progresses in electrocatalysts for water electrolysis, Electrochemical Energy Reviews 1 (2018) 483-530.

[18] R.F. Wang, H.W. F. Luo, S.J. Liao, Core–shell-structured low-platinum Eelectrocatalysts for fuel cell applications, Electrochemical Energy Reviews 1 (2018) 324-387.

[19] T. Vo, K. Purohit, C. Nguyen, B. Biggs, S. Mayoral, J.L. Haan, Formate: An energy storage and transport bridge between carbon dioxide and a formate fuel cell in a single device, ChemSusChem 8 (2015) 3853-3858.

[20] Y. S. Li, T. S. Zhao, A high-performance integrated electrode for anion-exchange membrane direct ethanol fuel cells, International Journal of Hydrogen Energy 36 (2011) 7707-7713.

[21] L. An, R. Chen, Direct formate fuel cells: A review, Journal of Power Sources 320 (2016) 127-139.

[22] C. Bianchini, V. ambagioni, J. Filippi, A. Marchionni, F. Vizza, P. Bert, A. Tampucci, Selective oxidation of ethanol to acetic acid in highly efficient polymer electrolyte membrane-direct ethanol fuel cells, Electrochemistry Communications 11 (2009) 1077-1080.

[23] L. An, T. S. Zhao, L. Zeng, X. H. Yan, Performance of an alkaline direct ethanol fuel cell with hydrogen peroxide as oxidant, International Journal of Hydrogen Energy 39 (2014) 2320 -2324.

[24] A. M. Bartrom, G. Ognibene, J. Ta, J. Tran, J. L. Haan, Catalysts for alkaline direct ethanol and direct formate fuel cells, ECS Transaction 50 (2012) 1913-1918.

[25] A. M. Bartrom, J. Ta, T. Q. Nguyen, J. Her, A. Donovan, J. L. Haan, Optimization of an anode fabrication method for the alkaline direct formate fuel cell, Journal of Power Sources 229 (2013) 234-238.

[26] T. Q. Nguyen, D. Minami, C. Hua, A. Miller, K. Tran, J. L. Haan, Ambient temperature operation of a platinum-free direct formate fuel cell, Journal of Fuel Cell Science and Technology 12 (2015) 014501.

[27] L. Zeng, Z. K. Tang, T. S. Zhao, A high-performance alkaline exchange membrane direct formate fuel cell, Applied Energy 115 (2014) 405-410.

[28] Y. S. Li, Y. Feng, X. D. Sun, Y. L. He, A sodium-ion-conducting direct formate fuel cell: generating electricity and producing base, Angewandte Chemie International Edition 56 (2017) 5734-5737.

[29] Y. S. Li, Y. L. He, W. W. Yang, A high-performance direct formate-peroxide fuel cell with palladium–gold alloy coated foam electrodes, Journal of Power Sources 278 (2015) 569-573.

[30] Y. S. Li, A liquid-electrolyte-free anion-exchange membrane direct formate-peroxide fuel cell, International Journal of Hydrogen Energy, 41 (2016) 3600-3604.

[31] Y. S. Li, H. Wu, Y. L. He, Y. Liu, L. Jin, Performance of direct formate-peroxide fuel cells, Journal of Power Sources 287 (2015) 75-80.

[32] T. S. Copenhaver, K. H. Purohit, K. Domalaon, L. Pham, B. J. Burgess, N. Manorothkul, V. Galvan, S. Sotez, F. A. Gomez, J. L. Haan, A microfluidic direct formate fuel cell on paper, Electrophoresis 36 (2015) 1825-1829.

[33] V. Galvan, K. Domalaon, C. Tang, S. Sotez, A. Mendez, M. Jalali‐Heravi, K. Purohit, L. Pham, J. Haan, F. A. Gomez, An improved alkaline direct formate paper microfluidic fuel cell, Electrophoresis 37 (2016) 504-510.

[34] L. An, R. Chen, Mathematical modeling of direct formate fuel cells, Applied Thermal Engineering 124 (2017) 232-240.

[35] A. K. Shukla, C. L. Jackson, K. Scott, R. K. Raman, An improved-performance liquid-feed solid-polymer-electrolyte direct methanol fuel cell operating at near-ambient conditions, Electrochimica Acta 47 (2002) 3401-3407.

[36] L. An, T. S. Zhao, Y. S. Li, Carbon-neutral sustainable energy technology: Direct ethanol fuel cells, Renewable and Sustainable Energy Reviews 50 (2015) 1462-1468.

[37] L. An, T. S. Zhao, Performance of an alkaline-acid direct ethanol fuel cell, International Journal of Hydrogen Energy 36 (2011) 9994-9999.

[38] L. Zhang, Q. Chang, H. Chen, M. Shao, Recent advances in palladium-based electrocatalysts for fuel cell reactions and hydrogen evolution reaction, Nano Energy 29 (2016) 198-219.

[39] L. An, T. S. Zhao, An alkaline direct ethanol fuel cell with a cation exchange membrane, Energy & Environmental Science 46 (2011) 2213-2217.

[40] K. R. Cooper, M. Smith, Electrical test methods for on-line fuel cell ohmic resistance measurement, Journal of Power Sources 160 (2006) 1088-1095.

[41] S. G. da Silva, J. C. M. Silva, G. S. Buzzo, E. V. Spinacé, A. O. Neto, M. H. M. T. Assumpção, PdAu/C electrocatalysts as anodes for direct formate fuel cell, Electrocatalysis 6 (2015) 442-446.

[42] H. I. Schlesinger, C. Coleman, Studies in conductivity. iii. Further studies on the behavior of the alkali metal formates in (anhydrous) formic acid, Journal of the American Chemical Society 38 (1916) 271-280.

[43] T. Q. Nguyen, A. M. Bartrom, K. Tran, J. L. Haan, Operation of the alkaline direct formate fuel cell in the absence of added hydroxide, Fuel Cells 13 (2013), 922-926.

[44] J. Kamcev, R. Sujanani, E. S. Jang, N. Yan, N. Moe, D. R. Paul, B. D. Freeman, Salt concentration dependence of ionic conductivity in ion exchange membranes, Journal of Membrane Science 547 (2018) 123-133.

[45] J. Prabhuram, T. S. Zhao, Z. X. Liang, H. Yang, and C. W. Wong, Pd and Pd-Cu alloy deposited nafion membranes for reduction of methanol crossover in direct methanol fuel cells, Journal of The Electrochemical Society 152 (2005) A1390-A1397.

[46] Y. B. Vassilyev, O. A. Khazova, N. N. Nikolaeva, Kinetics and mechanism of glucose electrooxidation on different electrode-catalysts: Part I. Adsorption and oxidation on platinum, Journal of Electroanalytical Chemistry and Interfacial Electrochemistry 196 (1985) 105-125.

[47] J. H. Kim, H. K. Kim, K. T. Hwang, J. Y. Lee, Performance of air-breathing direct methanol fuel cell with anion-exchange membrane, International Journal of Hydrogen Energy 35 (2010) 768-773.

[48] Y.S. Li, T.S. Zhao, W.W. Yang, Measurements of water uptake and transport properties in anion-exchange membranes, International Journal of Hydrogen Energy 35 (2010) 5656-5665.

[49] J. Chu, K. Lee, A. Kim, D. Yoo, Improved physicochemical stability and high ion transportation of poly (arylene ether sulfone) blocks containing a fluorinated hydrophobic part for anion exchange membrane applications, Polymers 10 (2018) 1400.

[50] E. Ivers-Tiffée, A. Weber, H. Schichlein, Electrochemical impedance spectroscopy, Handbook of Fuel Cells (2010).

Figure captions

Figure 1. Working principle of a passive direct formate fuel cell.

Figure 2. Design and fabrication of the passive direct formate fuel cell.

Figure 3. The polarization and power density curves.

Figure 4. The constant-current discharging behavior at a current density of 4.0 mA cm^{-2}.

Figure 5. Effect of the NaOH concentration on the fuel cell performance.

Figure 6. Effect of the NaOH concentration on the OCV and internal resistance.

Figure 7. Effect of the HCOONa concentration on the fuel cell performance.

Figure 8. Effect of the HCOONa concentration on the OCV and internal resistance.

Figure 9. Effect of the operating temperature on the fuel cell performance.

Figure 10. The constant-current discharging behaviors.

Figure 11. The Nyquist plots of electrochemical impedance spectra at various NaOH concentrations.

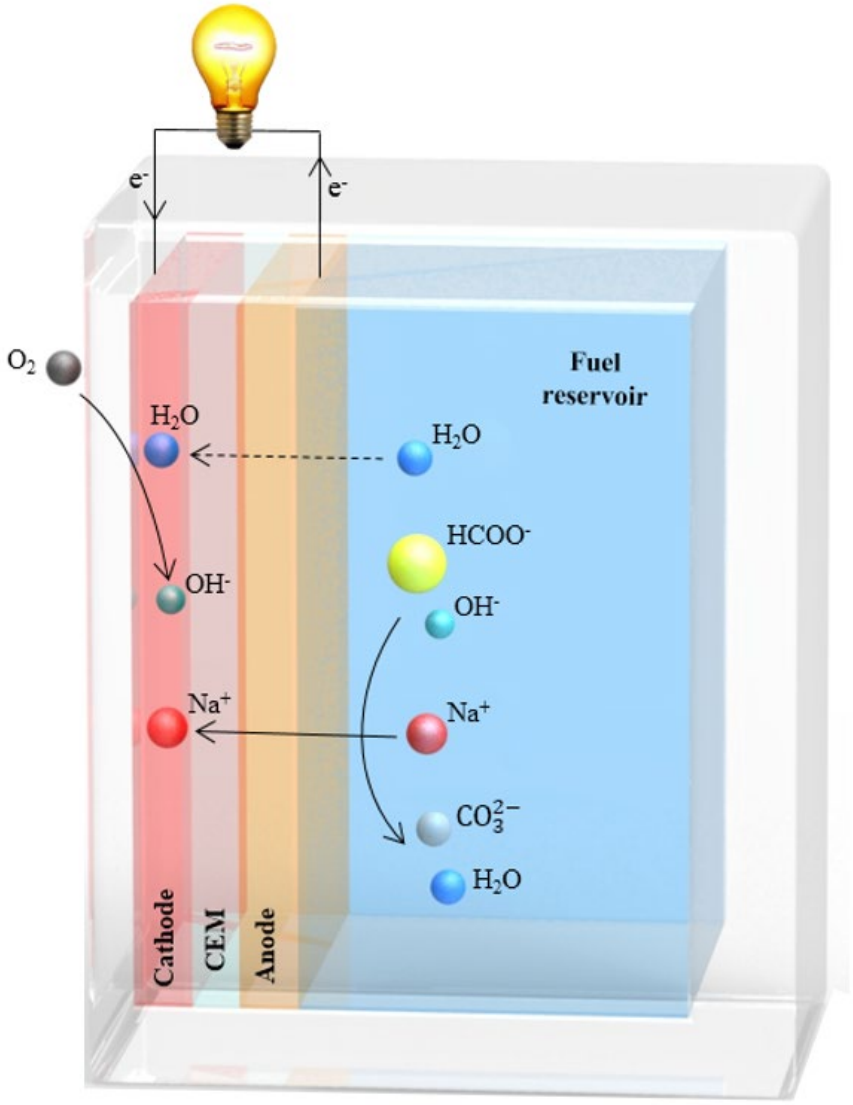

Figure 1. Working principle of a passive direct formate fuel cell.

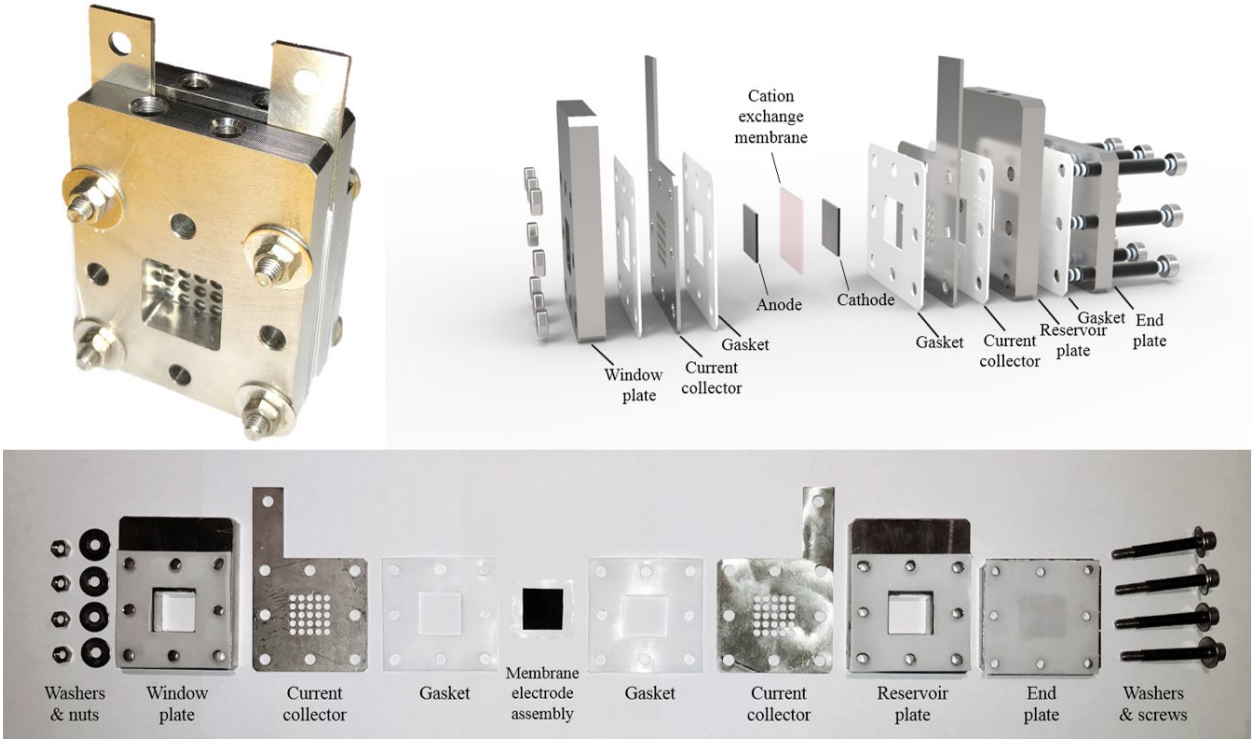

Figure 2. Design and fabrication of the passive direct formate fuel cell.

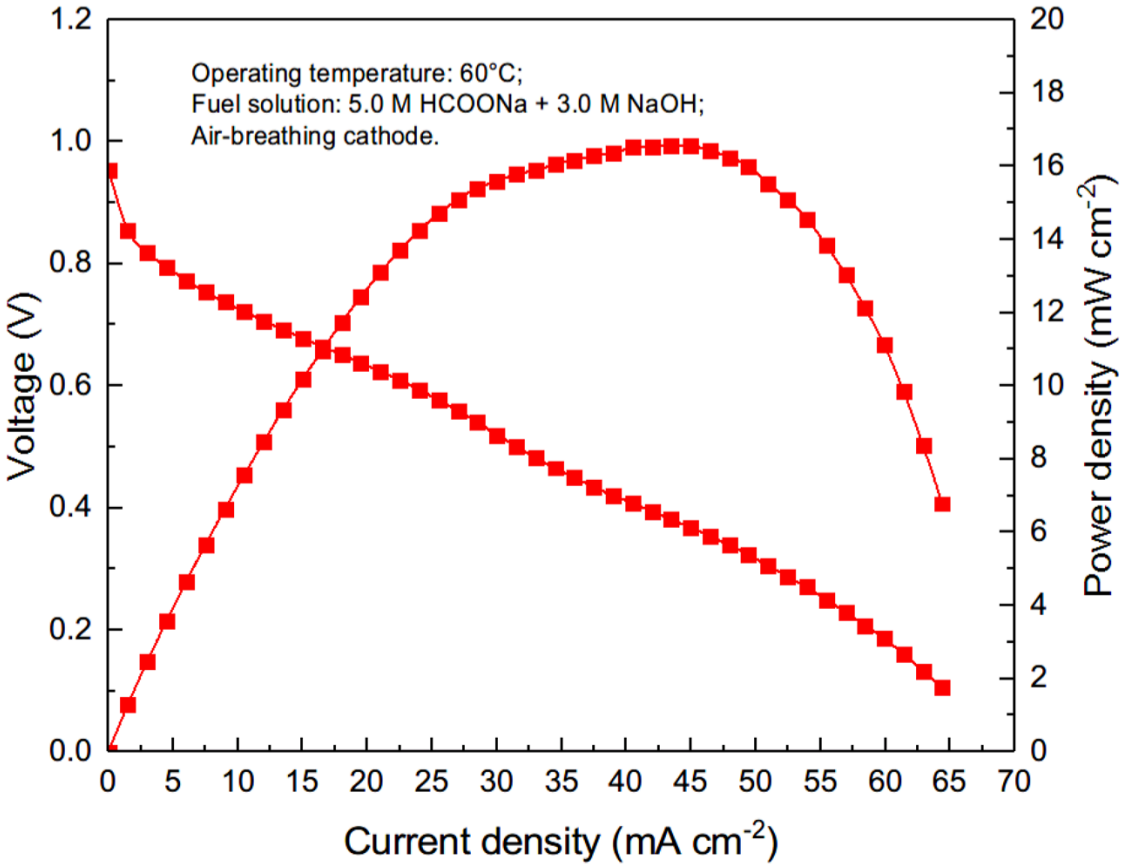

Figure 3. The polarization and power density curves.

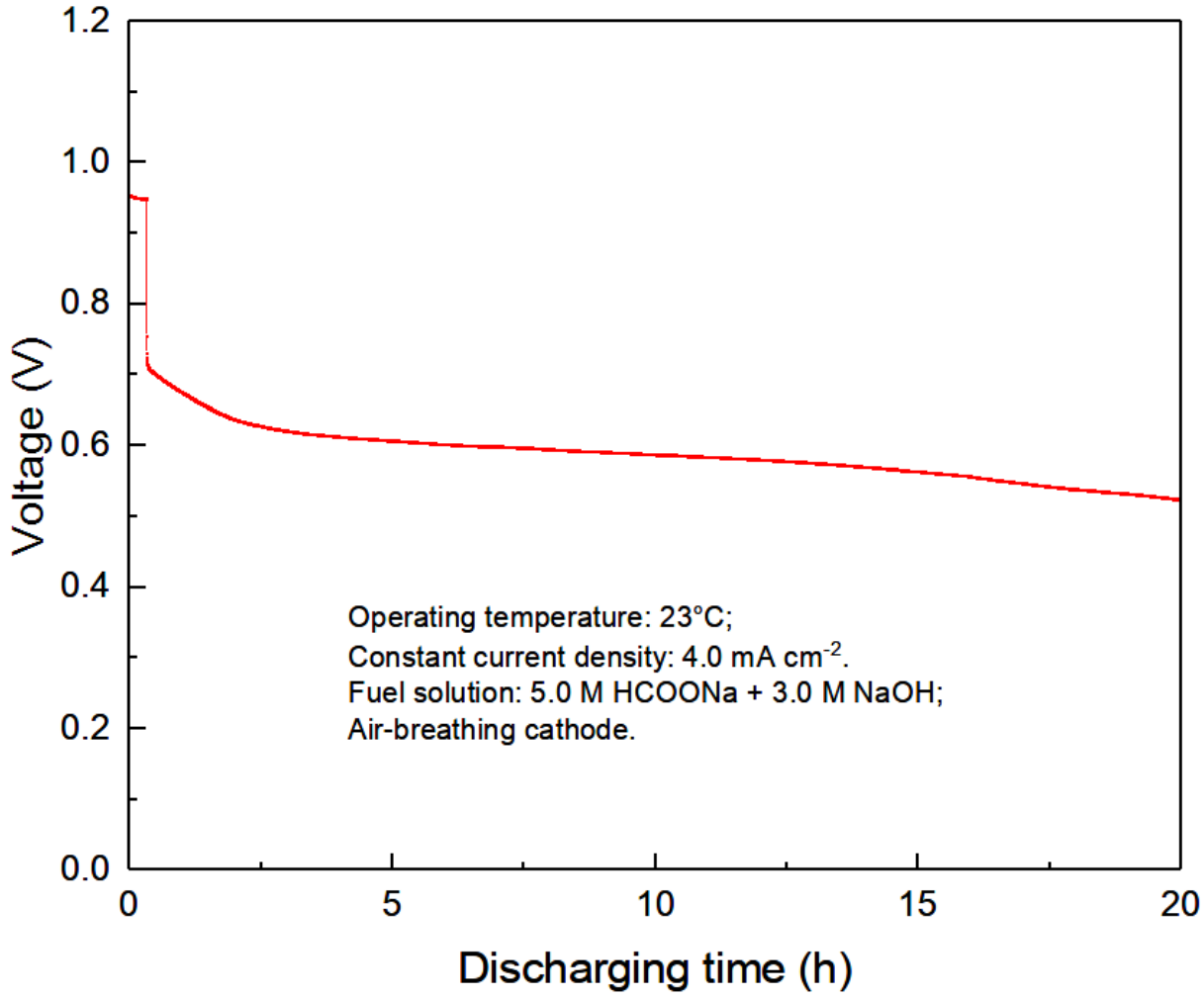

Figure 4. The constant-current discharging behavior at a current density of 4.0 mA cm^{-2}.

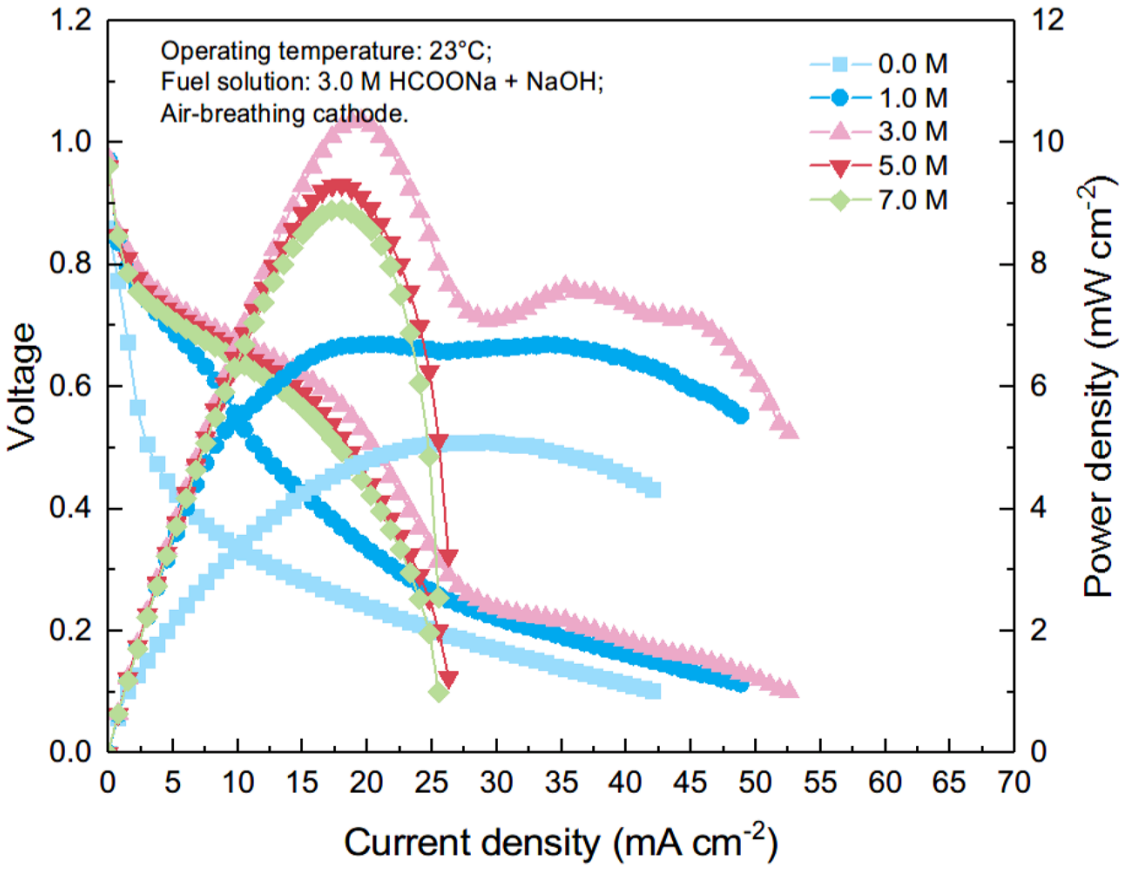

Figure 5. Effect of the NaOH concentration on the fuel cell performance.

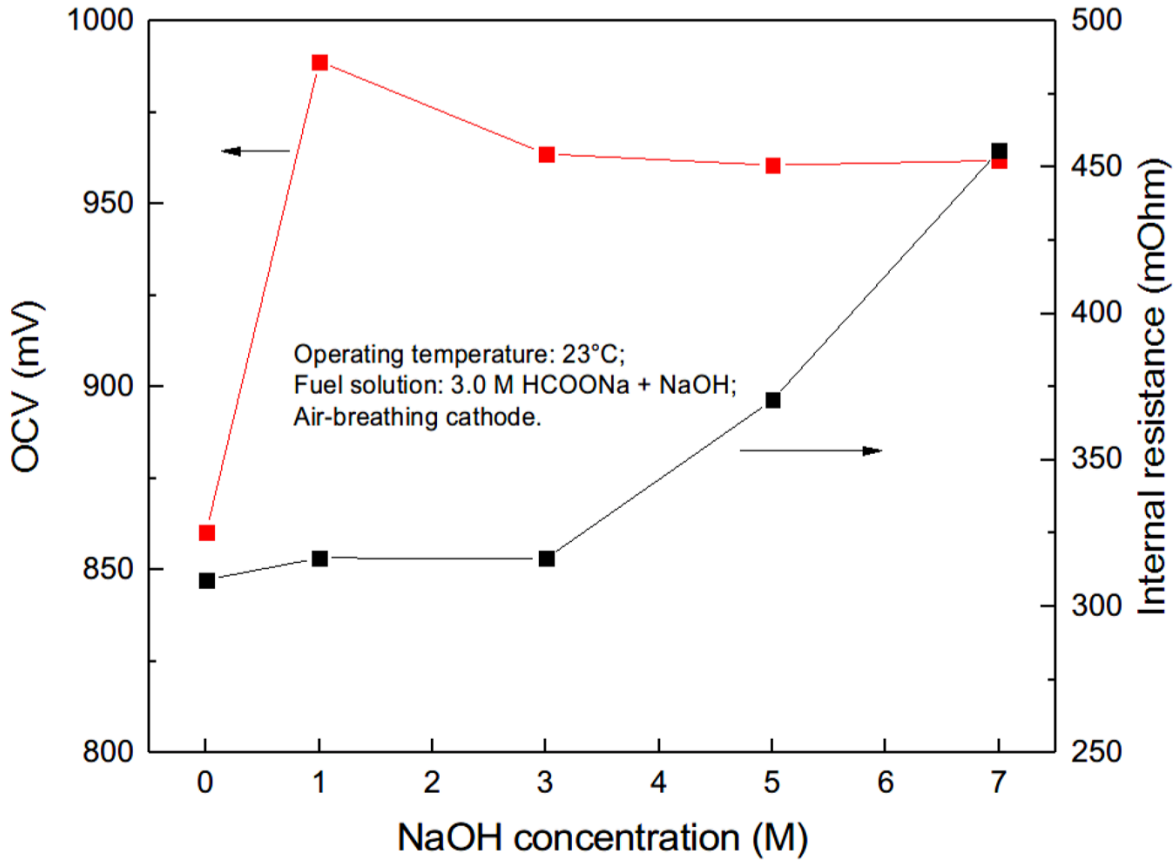

Figure 6. Effect of the NaOH concentration on the OCV and internal resistance.

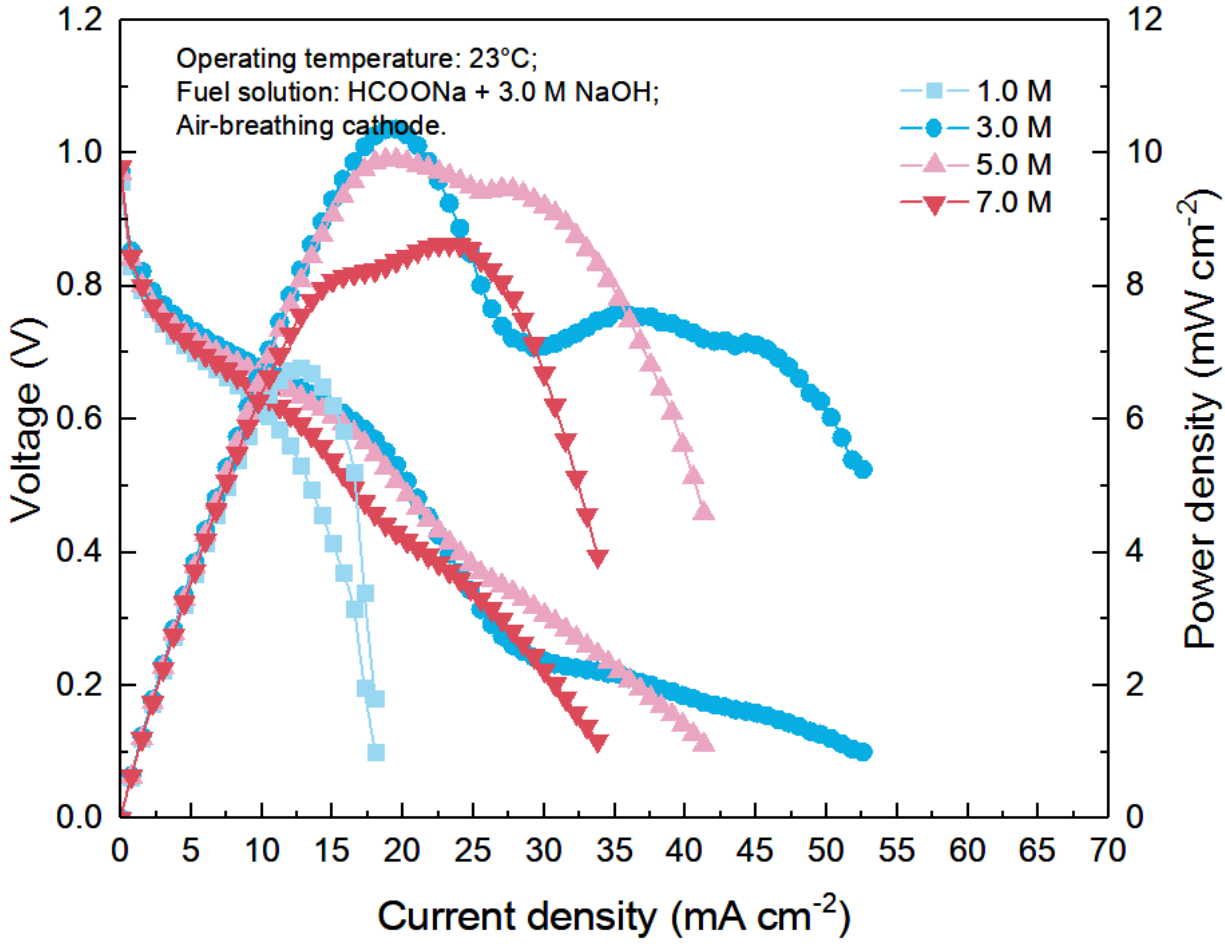

Figure 7. Effect of the HCOONa concentration on the fuel cell performance.

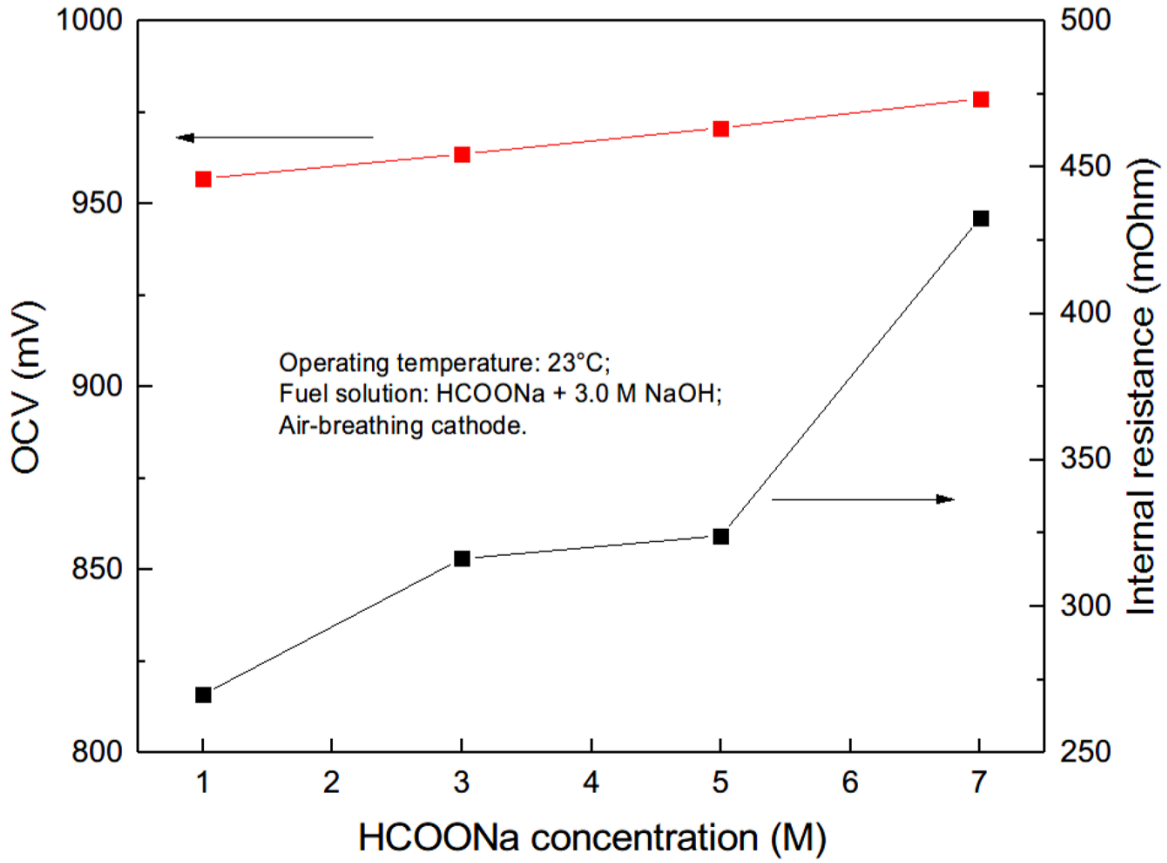

Figure 8. Effect of the HCOONa concentration on the OCV and internal resistance.

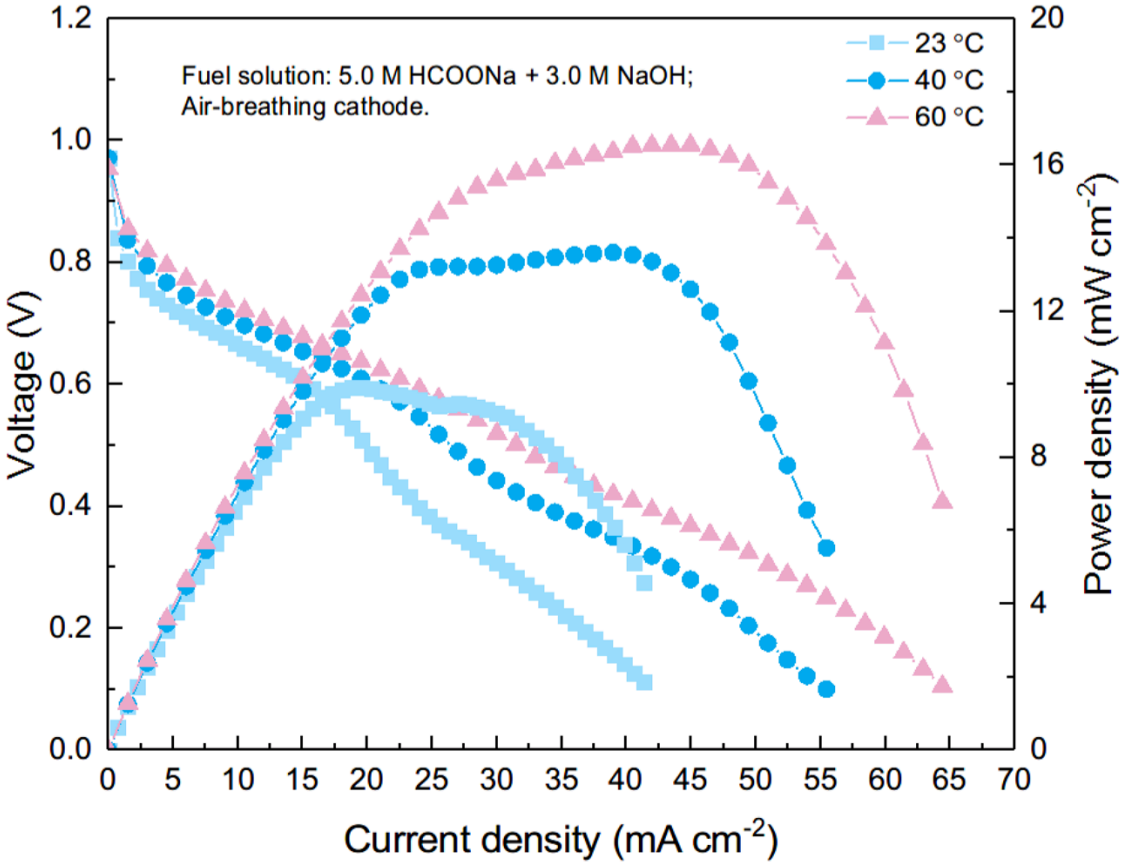

Figure 9. Effect of the operating temperature on the fuel cell performance.

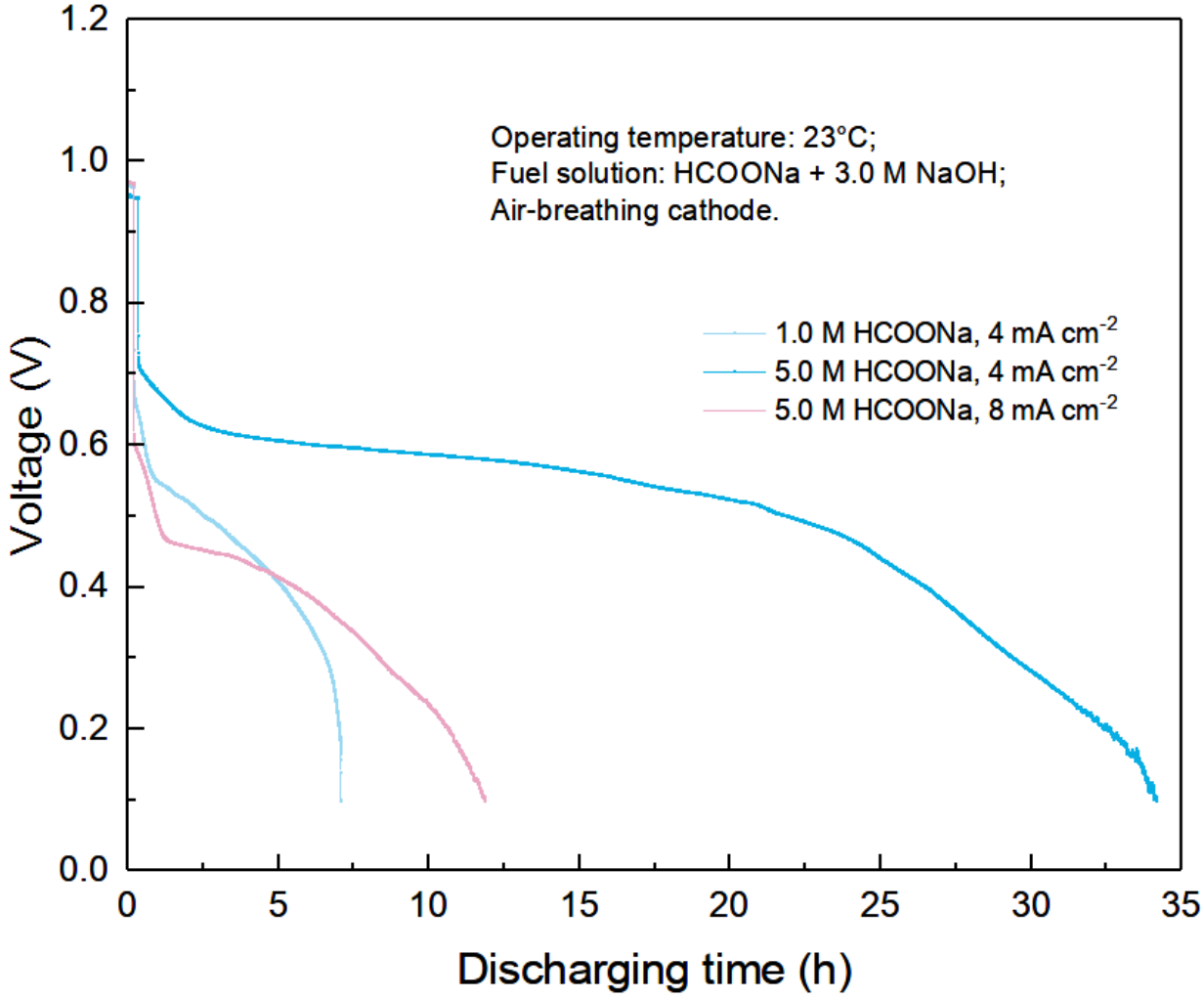

Figure 10. The constant-current discharging behaviors.

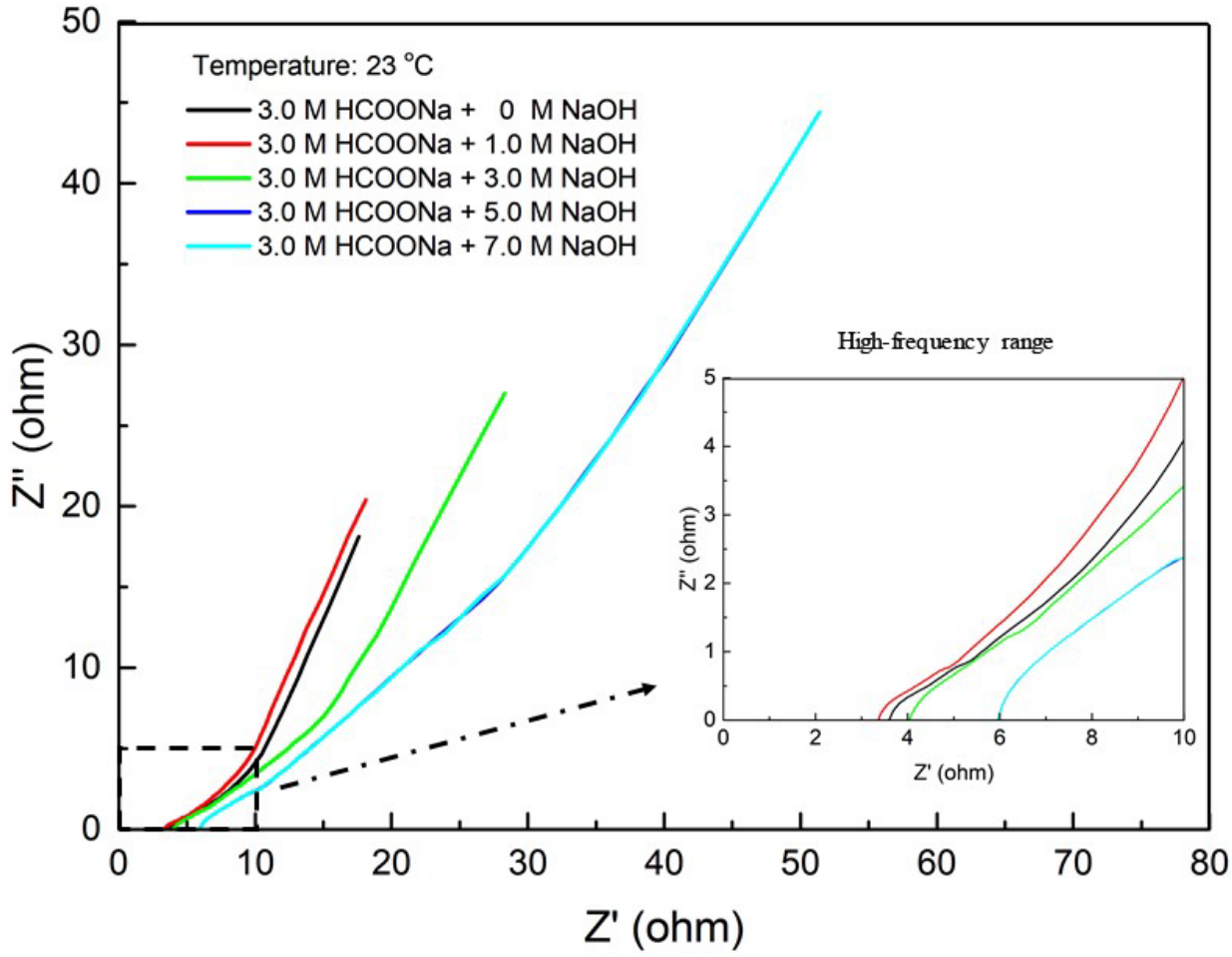

Figure 11. The Nyquist plots of electrochemical impedance spectra at various NaOH concentrations.